Journal of Molecular Catalysis A: Chemical 423 (2016) 293–299

Contents lists available at ScienceDirect

Journal of Molecular Catalysis A: Chemical

journal homepage: www.elsevier.com/locate/molcata

Molecular deposition of a macrocyclic cobalt catalyst on TiO_2 nanoparticles

Chao Liu [a], Tong Jin [a], Michael E. Louis [a], Sebastian A. Pantovich [a], Sarah L. Skraba-Joiner [a], Tijana Rajh [b,*], Gonghu Li [a,*]

[a] Department of Chemistry, University of New Hampshire, Durham, NH 03824, United States
[b] Center for Nanoscale Materials, Argonne National Laboratory, Argonne, IL 60439, United States

ARTICLE INFO

Article history:
Received 1 June 2016
Received in revised form 7 July 2016
Accepted 8 July 2016
Available online 9 July 2016

Keywords:
Hybrid photocatalyst
CO_2 reduction
Titanium dioxide
Cobalt cyclam

ABSTRACT

Hybrid photocatalysts consisting of molecular catalysts and solid-state surfaces have demonstrated great potential as robust and efficient systems in solar fuel production. Based on our prior work, we synthesized hybrid photocatalysts by depositing a macrocyclic Co(III) complex on three different TiO_2 nanomaterials via a microwave method. The hybrid photocatalysts were tested in CO_2 reduction and were thoroughly characterized with spectroscopic (UV–vis, FTIR and EPR) and microscopic (TEM) techniques. The presence of terminal OH groups on TiO_2 surfaces was essential for the molecular deposition of catalytically active Co(III) sites. On a TiO_2 material without such terminal OH groups, the Co(III) complex formed amorphous aggregates, which hindered interfacial electron transfer from photoactivated TiO_2 to the surface molecular complex. EPR studies further revealed important information regarding the coordination geometry and interaction with CO_2 of surface cobalt sites in the hybrid photocatalysts.

1. Introduction

Photocatalysis is a promising approach to harvest, convert, and store solar energy. For example, in photocatalytic CO_2 reduction, solar energy can be converted into chemical energy and stored in the form of chemical bonds [1,2]. Currently known photocatalysts for CO_2 reduction include molecular and supramolecular complexes [3–5] as well as inorganic semiconductors [6,7]. A key challenge for solar fuel production by CO_2 reduction is the lack of photocatalytic systems that are both highly efficient and robust under photochemical conditions. In recent years, hybrid photocatalysts combining molecular catalysts with solid-state surfaces have attracted extensive interests from researchers in the field of solar fuels [8–10]. Such hybrid photocatalysts generally demonstrate enhanced solar conversion efficiency and improved photostability. In this report, we investigate a rare example of hybrid photocatalysts featuring photo-induced electron transfer from titanium dioxide (TiO_2) to a surface molecular catalyst.

In hybrid systems for solar CO_2 reduction, molecular catalysts are covalently attached to solid-state surfaces [9–12], incorporated in frameworks/porous environment [13–16] or confined to surfaces by polymerization [17,18]. Typical solid-state surfaces for molecular CO_2-reduction catalysts include periodic mesoporous organosilicas, metal-organic frameworks, and inorganic semiconductors. For example, Takeda and co-workers prepared a hybrid photocatalyst by covalently attaching a tricarbonyl Re(I) complex on a light-absorbing mesoporous organosilica [16]. Enhanced CO_2-to-CO conversion was achieved upon UV light activation of the organosilica and subsequent resonance energy transfer to the Re(I) catalytic centers. In addition, the mesoporous structure protected the molecular Re(I) complex against photochemical decomposition [16]. Similar effects of catalyst heterogenization were observed in photocatalytic CO_2 reduction using a Re(I) catalyst incorporated in a light-absorbing metal-organic framework [19].

Inorganic semiconductors such as TiO_2 have been utilized as the solid-state support for several molecular CO_2-reduction catalysts [20–26]. Windle and co-workers synthesized a hybrid Re(I) photocatalyst by grafting a molecular Re(I) complex onto TiO_2 through phosphate groups [24]. The surface immobilization significantly improved photocatalytic activity of the Re(I) complex in CO_2 reduction under visible-light irradiation, which activates the Re(I) complex but not the TiO_2 support. The researchers utilized transient absorption spectroscopy to demonstrate increased lifetime of a reduced Re(I) intermediate on the TiO_2 surface. It was suggested that the longer-lived anionic Re(I) species on TiO_2 has a

* Corresponding authors.
E-mail addresses: rajh@anl.gov (T. Rajh), gonghu.li@unh.edu (G. Li).

http://dx.doi.org/10.1016/j.molcata.2016.07.019
1381-1169/

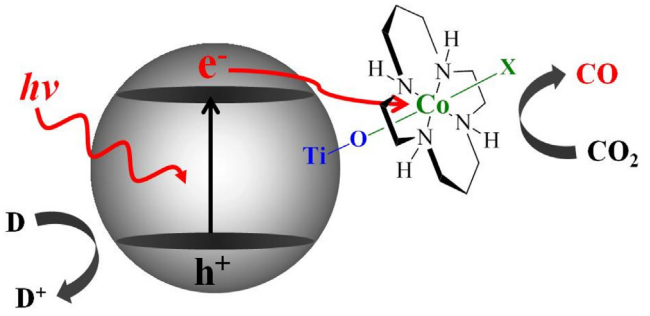

Fig. 1. Schematic of the hybrid Co(III) photocatalyst. D is an electron donor. X = OH or Cl.

greater probability of reacting with CO_2 and undergoing the second reduction required for the production of CO [24].

Recently, we prepared a hybrid photocatalyst by depositing a molecular Co(III) complex, [Co(cyclam)Cl_2]Cl where cyclam is 1,4,8,11-tetraazacyclotetradecane, onto TiO_2 (Fig. 1) [21]. The hybrid photocatalyst was photoactive in CO_2 reduction in the presence of sacrificial electron donors. The molecular Co(III) complex was also grafted onto a mesoporous silica for use in photocatalytic CO_2 reduction in the presence of a molecular photosensitizer [27]. The best catalytic activity was achieved when the surface Co(III) complex formed a monolayer in the silica mesopores.

In this work, we build on prior work to demonstrate the importance of molecular deposition in achieving photo-induced electron transfer from TiO_2 to the molecular catalyst for CO_2 reduction in the presence of an electron donor. We synthesize three hybrid photocatalysts using different TiO_2 nanomaterials via a microwave method. We further investigate the hybrid photocatalysts using spectroscopic and microscopic techniques, including UV–vis, Fourier Transform infrared (FTIR) and electron paramagnetic resonance (EPR) spectroscopies, and transmission electron microscopy (TEM). Through these studies, we identify surface characteristics that are key to the molecular deposition of the molecular catalyst, and further investigate coordination geometry of the surface metal sites and their interaction with CO_2.

2. Experimental section

2.1. Materials

Triethylamine (TEA, ≥99%), triethanolamine (TEOA, ≥99%), acetonitrile (99.999%), hydrochloric acid (37%), and 1,4,8,11-tetraazacyclotetradecane (cyclam, 98%) were obtained from Sigma-Aldrich. Methanol (99.9%) was purchased from Fisher Scientific. Cobalt(II) chloride hexahydrate was obtained from J.T. Baker. *N,N*-dimethylformamide (DMF, 99.8%) was obtained from Acros Organics. Ethanol (95.0%) and chloroform (99.8%) were purchased from Parmo Products Inc. All reagents were used without further purification. P25 TiO_2 (specific surface area 57 m^2/g, phase composition ~80% Anatase and ~20% Rutile, see Fig. S1 in Electronic Supplementary information) was obtained from Evonik and used as received. Anatase TiO_2 nanopowder (99.7% trace metal basis, specific surface area 56 m^2/g) and Rutile TiO_2 nanopowder (99.5% trace metal basis, specific surface area 20 m^2/g) were obtained from Sigma-Aldrich and used as received.

2.2. Catalyst synthesis

Hybrid photocatalysts were synthesized by a microwave method (Fig. 2). In a typical synthesis, 100 mg TiO_2 was mixed with 10 mg [Co(cyclam)Cl_2]Cl and 65 μl triethylamine in 15 ml acetonitrile. The presence of triethylamine was found to be essential for the successful deposition of the Co(III) catalyst on TiO_2 via reacting with surface Ti—OH groups. The mixture in a capped reaction vessel was placed in a CEM Discover single-mode microwave reactor and underwent reaction for 120 min at 80 °C. After the microwave reaction, the resulting brownish precipitate was recovered by centrifugation, and washed twice with chloroform and twice with ethanol. After drying at room temperature, the hybrid photocatalyst was obtained as a light brownish powder. Our previous results [21] clearly indicated that the molecular structure of Co^{III}(cyclam) was retained upon deposition on TiO_2 surfaces, with some of the Cl ligands replaced by OH groups (Fig. 2).

Following this microwave synthesis, three hybrid photocatalysts were prepared in the presence of P25, Anatase and Rutile TiO_2 nanomaterials. The three hybrid photocatalysts are denoted as Co^{III}(cyclam)X/P25, Co^{III}(cyclam)X/Anatase, and Co^{III}(cyclam)X/Rutile. Catalyst loadings were determined by elemental analysis to be 59, 63, and 88 μmol Co per gram of Co^{III}(cyclam)X/P25, Co^{III}(cyclam)X/Anatase, and Co^{III}(cyclam)X/Rutile, respectively. The loadings were used to calculate turnover numbers (TONs) in photocatalysis.

2.3. Catalyst characterization

Elemental analysis was conducted by acid digestion of powder samples, followed by quantification using a Varian Vista AX induced coupled plasma atomic emission spectrometer. Transmission electron microscopy images were taken on a Zeiss/LEO 922 Omega system. UV–vis spectra were obtained on a Cary 50 Bio spectrophotometer. A Barrelino diffuse reflectance probe was used to collect UV–vis spectra of powder samples using $BaSO_4$ as a standard. FTIR spectra were collected on a Thermo Nicolet 6700 FTIR spectrometer using a Harrick Praying Mantis diffuse reflectance accessory (for powder samples) or a transmission cell (for gaseous samples). EPR spectra were collected on a Bruker ELEXSYS E580 spectrometer operating in the X-band (9.4 GHz) mode and equipped with an Oxford CF935 helium flow cryostat. Spectra of powder samples were collected under N_2 at liquid He temperature. For the studies of CO_2 adsorption, the samples were purged with CO_2 at room temperature, cooled to liquid He temperature, and illuminated in the EPR cavity using a 300 W Xe lamp (PerkinElmer) with 400 nm long-pass and water as IR cutoff filters.

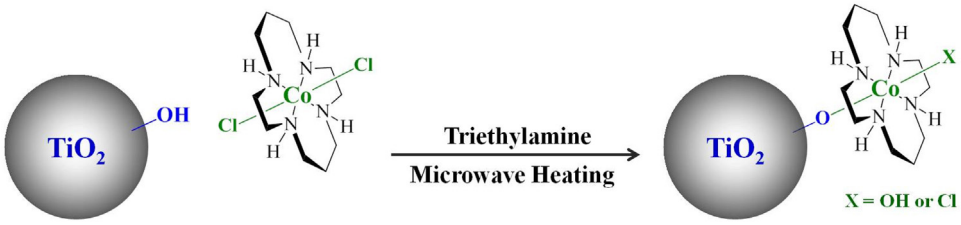

Fig. 2. Synthesis of the hybrid photocatalyst in the presence of triethylamine (TEA).

2.4. Photocatalytic CO_2 reduction

In photocatalytic CO_2 reduction, 1 mg of photocatalyst in the powder form was dispersed in a 4.0-ml acetonitrile solution containing TEOA (acetonitrile: TEOA = 3:1 v/v) in a Pyrex test tube. Prior to photocatalytic testing, the reaction solution was bubbled with CO_2 (99.999%, Airgas) in the dark for 20 min. The reaction solution was then irradiated with a 200-W Hg lamp equipped with a water filter. Light intensity on the reaction solution was fixed at 100 mW/cm^2. The head space above the reaction solution was sampled with a gas-tight syringe at different time intervals for product analysis using an Agilent 7820 GC equipped with a TCD detector. Production of formic acid in reaction solutions was monitored by NMR.

3. Results and discussion

3.1. Photocatalysis

Heterogeneous photocatalysts based on TiO_2 materials have been extensively investigated in CO_2 reduction since the early work by Inoue and co-workers [28–32]. Compared to molecular catalysts, semiconductor photocatalysts are relatively stable and inexpensive. However, multi-electron processes, including CO_2-reduction catalysis, on TiO_2 surfaces are extremely inefficient due to recombination of photoexcited charge carriers (electrons and holes) [33–38]. Instead, efficient solar energy conversion has been achieved by surface functionalization of TiO_2 nanomaterials with coordination complexes such as Ru(II)-based dye molecules. In dye-sensitized solar cells [39–43] and photosynthesis cells [44–49], TiO_2 serves to accept photoexcited electrons from the surface coordination complexes upon interfacial electron transfer. The success of surface dye sensitization has inspired design of hybrid photocatalysts consisting of TiO_2 and surface molecular catalysts [24,25,50,51]. In this study, we utilize TiO_2 as a solid-state photosensitizer for [Co(cyclam)Cl_2]Cl, which is as a molecular CO_2-reduction catalyst based on an earth-abundant metal. This Co(III) complex demonstrated excellent activity and selectivity in reducing CO_2 to CO in the presence of molecular photosensitizers, including *p*-terphenyl, under UV irradiation [52,53].

The three hybrid photocatalysts, Co^{III}(cyclam)X/P25, Co^{III}(cyclam)X/Anatase, and Co^{III}(cyclam)X/Rutile, were evaluated in photocatalytic CO_2 reduction in the presence of triethanolamine (TEOA) as a sacrificial electron donor. Co^{III}(cyclam)X/P25 and Co^{III}(cyclam)X/Anatase exhibited very good activity in photocatalytic CO_2 reduction, while negligible CO production was observed using Co^{III}(cyclam)X/Rutile (Fig. 3). Hydrogen gas (CO/H_2 ~1) as a byproduct was produced using the hybrid photocatalysts.

In our study, products in the gas phase were analyzed with a GC. Product detection in the solution phase by NMR indicated no significant production of formate after photocatalysis. In order to rule out the possibility of CO generation from carbon residues on the synthesized samples, products in the gas phase were also analyzed with FTIR spectroscopy in combination with isotope labeling. Fig. 4 displays the FTIR spectrum of the head-space gases above a reaction solution after photocatalytic reduction of $^{13}CO_2$ by Co^{III}(cyclam)X/P25 under UV irradiation. In the spectrum, the rotational-vibrational band of gaseous ^{13}CO centered at 2096 cm^{-1} clearly confirms the production of CO from CO_2 on the hybrid photocatalyst.

Under the experimental conditions employed in this study (TEOA, CO_2 atmosphere, and UV irradiation), no CO was produced by any of the following: (i) P25 TiO_2 nanoparticles, (i) [Co(cyclam)Cl_2]Cl and P25, or (iii) Co^{III}(cyclam)X/SiO_2 prepared by depositing the Co(III) complex on a fumed silica following the microwave synthesis. In addition, no CO formation was observed using Co^{III}(cyclam)X/P25 under visible-light irradiation ($\lambda > 420$ nm) which cannot activate P25 TiO_2. Therefore, in this hybrid Co^{III}(cyclam)X/TiO_2 system the surface Co(III) complex is the catalyst for CO_2 reduction while TiO_2 nanoparticles function as the light-harvesting support (Fig. 1).

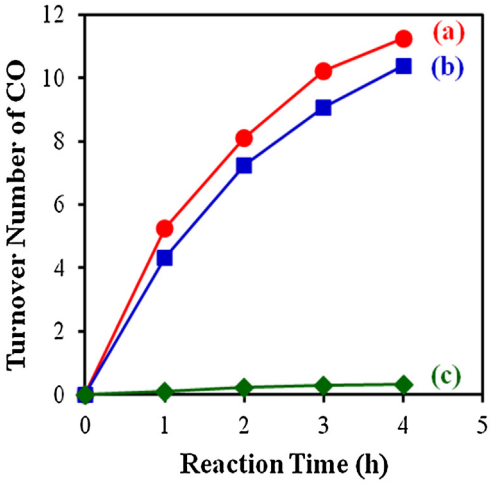

Fig. 3. CO production in photocatalytic CO_2 reduction using (a) Co^{III}(cyclam)X/P25, (b) Co^{III}(cyclam)X/Anatase, and (c) Co^{III}(cyclam)X/Rutile. Reaction conditions: UV irradiation, TEOA as sacrificial electron donor. Turnover numbers were calculated based on the amount of CO produced per mole of Co in the reaction suspension.

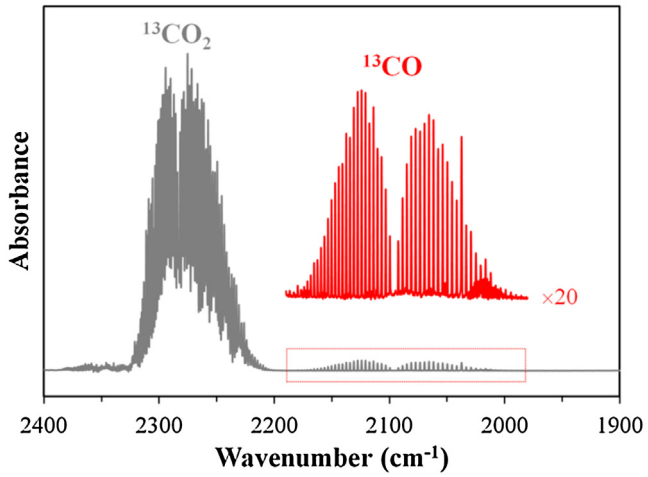

Fig. 4. FTIR spectrum of gases in the head space above a reaction solution after photocatalytic reduction of $^{13}CO_2$ by Co^{III}(cyclam)X/P25 under UV irradiation for 6 h. See Fig. S2 for experimental details.

3.2. FTIR spectroscopy

Further surface chemistry studies also indicate that CO_2 reduction occurs on the surface Co(III) sites. In the surface chemistry studies, a hybrid photocatalyst in the powder form was placed in a diffuse reflectance accessory and exposed to an atmosphere of CO_2. Photocatalysis at the gas-surface interface was carried out in the absence of any solvent or TEOA. The photocatalyst surface was monitored with *in situ* infrared detection [54,55]. At various stages during photocatalysis, difference FTIR spectra were obtained by subtracting spectra acquired prior to photocatalysis from corresponding spectra collected after UV irradiation. Therefore, the difference spectra provide information regarding changes on the photocatalyst surface upon light irradiation. The formation

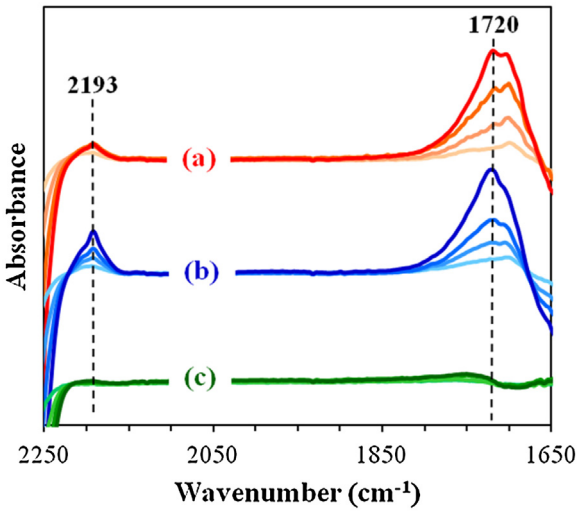

Fig. 5. Difference FTIR spectra obtained after photocatalysis at the gas-surface interface using (a) Co^{III}(cyclam)X/P25, (b) Co^{III}(cyclam)X/Anatase, and (c) Co^{III}(cyclam)X/Rutile. For each sample, spectra were collected after UV irradiation for 5, 15, 30, 60 min (bottom to top).

of CO was observed on surface Co(III) sites in Co^{III}(cyclam)X/P25 and Co^{III}(cyclam)X/Anatase, as indicated by the infrared bands at 2193 cm^{-1} in the spectra shown in Fig. 5 (a and b) [56]. The formation of surface carbonate species (1720 cm^{-1}) was also observed on these two samples. Negligible changes were observed on Co^{III}(cyclam)X/Rutile during photocatalysis (Fig. 5c). The comparison shown in Fig. 5 is in excellent agreement with photocatalysis in the solution phase (Fig. 3). Under the same experimental conditions, surface CO species was not observed on bare P25 TiO_2 [21], further confirming the key role of surface Co(III) sites in mediating CO_2-reduction catalysis.

These photocatalysis results clearly indicate photoexcited electron transfer from the TiO_2 conduction band to the surface Co(III) catalyst for CO_2 reduction in the presence of a sacrificial electron donor. In our previous studies, reduction potentials of the Co^{III}/Co^{II} and Co^{II}/Co^{I} redox couples for Co^{III}(cyclam)X were measured to be −0.21 V and −0.93 V vs NHE, respectively [21]. Therefore, photoexcited electrons in the TiO_2 conduction band (potential ∼ −0.6 V vs NHE at pH = 7) [57] are not energetic enough to reduce Co(II) to Co(I) needed to catalyze CO_2-to-CO conversion (−0.53 V *vs.* NHE). The exact driving force for the photoexcited electron transfer is unclear. However, we note that the reduction potential of Co^{II}/Co^{I} is largely dependent of coordination ligands. For example, the reduction potential of Co^{II}/Co^{I} for [Co(cyclam)Cl_2]Cl was −1.39 V vs NHE, in comparison to −0.93 V vs NHE for Co^{III}(cyclam)X [21]. The Ti—O—Co linkage in our hybrid photocatalysts (Fig. 1) and the presence of excess TEOA in reaction solutions could further alter the redox properties of the Co^{III}(cyclam) unit on TiO_2 surfaces under photochemical conditions. The importance of such surface Ti—O—Co linkage is further described in the following spectroscopic and microscopic studies.

3.3. UV–vis spectroscopy

As shown in Fig. 3, the hybrid photocatalyst prepared on the Rutile nanopowder demonstrated much lower activity than Co^{III}(cyclam)X/P25 and Co^{III}(cyclam)X/Anatase. In many photocatalytic applications using bare TiO_2 materials, the rutile phase is generally considered less active than the anatase phase due to more significant charge recombination in rutile [29]. However, the particular Rutile nanopowder employed in our study is more active than the Anatase nanopowder in photocatalytic degradation of methylene blue (Fig. S3), despite its lower surface area. Therefore, the difference in charge carrier dynamics is not responsible for the observed difference in photocatalytic activity shown in Fig. 3.

In the UV–vis spectra of Co^{III}(cyclam)X/P25 and Co^{III}(cyclam)X/Anatase, two broad absorptions are seen at ∼450 nm and 600 nm, indicating the presence of macrocyclic Co(III) complex (Fig. 6a and b) [21]. However, these features are not distinguishable in the spectrum of Co^{III}(cyclam)X/Rutile (Fig. 6c). Therefore, the state of Co^{III}(cyclam)X on the Rutile material is different from that on P25 and Anatase. Such difference might account for the observed photocatalytic activity displayed in Fig. 3. Furthermore, there is no significant amount of cobalt oxides, which would exhibit distinguishable peaks at 530, 595, and 655 nm [27], in the synthesized photocatalysts.

3.4. Transmission electron microscopy

In combination with UV–vis spectroscopic studies, microscopic investigation of the hybrid photocatalysts indicates that Co^{III}(cyclam)X is molecularly deposited as a thin layer on P25 and Anatase surfaces. Only TiO_2 nanoparticles are observed in the TEM images of Co^{III}(cyclam)X/P25 and Co^{III}(cyclam)X/Anatase (Fig. 7a and b). Close inspection of the TEM images indicates that no separate phase is present in either of these two samples. In comparison, amorphous, nano-sized particles are seen in the TEM image of Co^{III}(cyclam)X/Rutile (Fig. 7c). These particles are either attached to

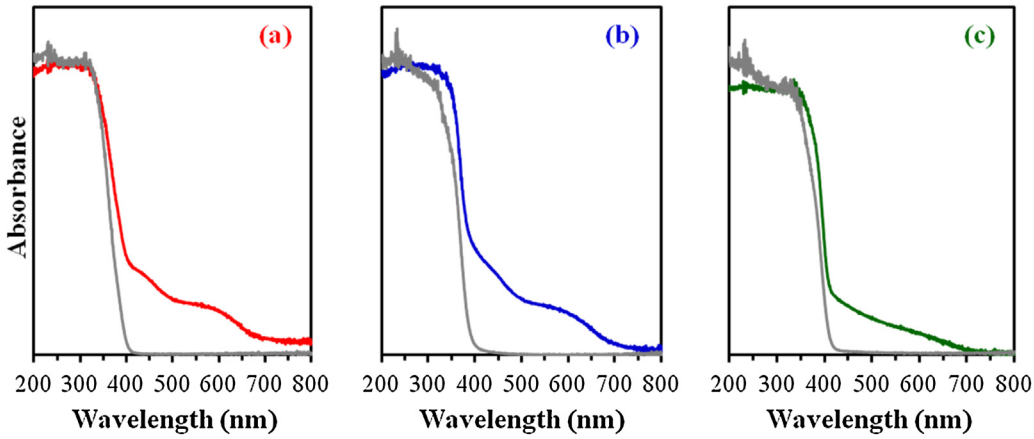

Fig. 6. UV–vis spectra of (a) Co^{III}(cyclam)X/P25, (b) Co^{III}(cyclam)X/Anatase, and (c) Co^{III}(cyclam)X/Rutile. The spectra of corresponding bare TiO_2 materials are also plotted (gray).

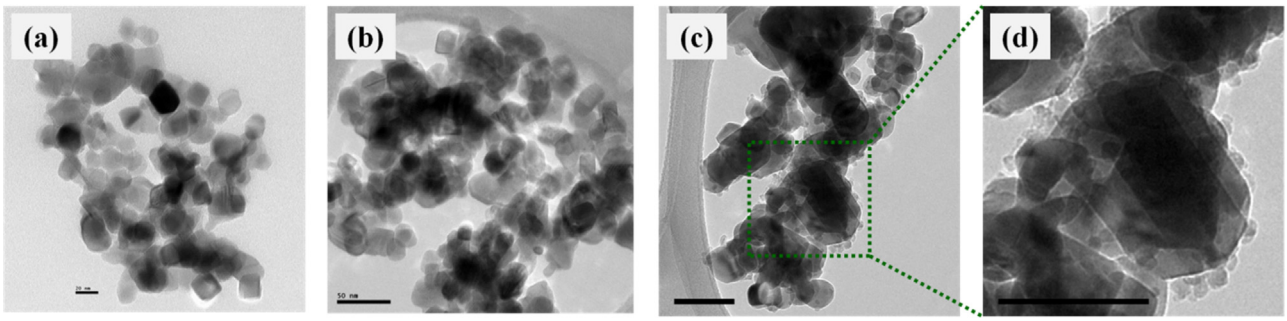

Fig. 7. TEM images of (a) Co^{III}(cyclam)X/P25, (b) Co^{III}(cyclam)X/Anatase, and (c, d) Co^{III}(cyclam)X/Rutile. Scale bars are (a) 20 nm, (b) 50 nm, and (c, d) 100 nm.

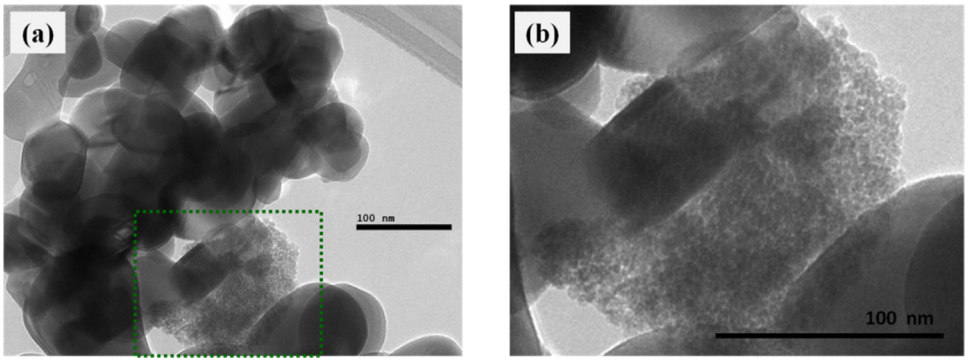

Fig. 8. TEM images of Co^{III}(cyclam)X/Rutile. Image (b) is an enlarged view of the highlighted area in image (a). Scale bars are 100 nm.

the Rutile nanoparticles (Fig. 7d) or form large aggregates (Fig. 8). Further comparison with the TEM image of bare Rutile confirms that these amorphous particles are Co^{III}(cyclam)X in the solid state that formed during the synthesis of Co^{III}(cyclam)X/Rutile.

Previously we have found that surface Ti—OH groups are important for successful deposition of active Co(III) catalysts on TiO_2 nanoparticles via a reflux method [21]. Similar results were obtained for the three hybrid photocatalysts prepared by the microwave method in this study. Infrared studies of the hybrid photocatalysts show that the Rutile surface lacks terminal Ti—OH groups associated with a band at 3632 cm^{-1} (Fig. S4) for effective deposition of Co^{III}(cyclam)X. According to the UV–vis and TEM results (Figs. 6–8), Co^{III}(cyclam)X is molecularly deposited as a thin layer on P25 and Anatase surfaces but forms aggregates on Rutile. In the study by Petsi and co-workers [58], both bridging and terminal OH groups were found to be important for the deposition of $[Co(H_2O)_6]^{2+}$ on TiO_2 nanoparticles. In our study, the presence of terminal OH group associated with the infrared absorption at 3632 cm^{-1} is essential for the molecular deposition of catalytically active Co^{III}(cyclam)X on P25 and Anatase surfaces via Ti—O—Co linkages (Fig. 1).

Based on the specific surface areas of the TiO_2 nanomaterials and elemental analysis results, surface catalyst densities are estimated to be 6–7 Co per nm^2 surface area in Co^{III}(cyclam)X/P25 and Co^{III}(cyclam)X/Anatase, and ~26 Co per nm^2 surface area in Co^{III}(cyclam)X/Rutile. These numbers further support our conclusion that Co^{III}(cyclam)X is molecularly deposited on P25 and Anatase surfaces. The absence of terminal OH groups for effective deposition of Co^{III}(cyclam)X on the Rutile material resulted in the formation of Co^{III}(cyclam)X in the aggregated form as observed in Figs. 7 and 8. The lack of sufficient Ti—O—Co linkages in Co^{III}(cyclam)X/Rutile can be used to explain inefficient photoexcited electron transfer from Rutile to surface Co^{III}(cyclam)X, which led to its poor activity in photocatalytic CO_2 reduction (Fig. 3).

An infrared band at 3670 cm^{-1}, associated with bridging Ti—OH groups, is also present in the spectra of the three TiO_2 samples (Fig. S4). This infrared band disappeared in the spectra of the three hybrid photocatalysts, indicating that deposition of Co^{III}(cyclam)X also occurred through reacting with the bridging Ti—OH groups. However, comparison shown in Figs. 4–7 suggests that catalyst deposition through these bridging Ti—OH groups didn't allow photoexcited electron transfer from TiO_2 to surface Co^{III}(cyclam)X.

3.5. EPR spectroscopy

Characterization with EPR spectroscopy further supports the fact that surface cobalt sites exist in different states on Rutile than on P25 and Anatase surfaces. Although the Co(III) compound itself is EPR silent, some paramagnetic Co(II) species and radicals are present in the synthesized hybrid photocatalysts, as indicated by the following EPR results. This is similar to the study by Kohno and co-workers [59], in which paramagnetic Co(II) species were found to be trapped in single crystals of a Co(III) compound. The presence of paramagnetic Co(II) species is likely a consequence of the use of triethylamine in the synthesis of our hybrid photocatalysts.

The EPR spectra of Co^{III}(cyclam)X/P25 and Co^{III}(cyclam)X/Anatase are almost identical, except for a dark signal in the latter due to trace metal impurity in the Anatase nanopowder (Fig. S5). Therefore, the spectra of Co^{III}(cyclam)X/P25 and Co^{III}(cyclam)X/Rutile are chosen for comparison in this section. In the spectrum of Co^{III}(cyclam)X/P25 under N_2 (Fig. 9a, gray trace), resonances corresponding to mononuclear high-spin Co(II) ($S = 3/2$) centers are observed at $g_x = 5.89, g_y = 3.40$, and $g_z = 2.22$ (not labeled). The same spectrum also contains resonances near $g = 2$ (not labeled) that are associated with trapped electrons and holes [33,34] in P25 upon exposure to ambient light (Fig. S6). In the spectrum of Co^{III}(cyclam)X/Rutile (Fig. 9b, gray trace), however, a very different EPR spectrum is observed in the high-spin

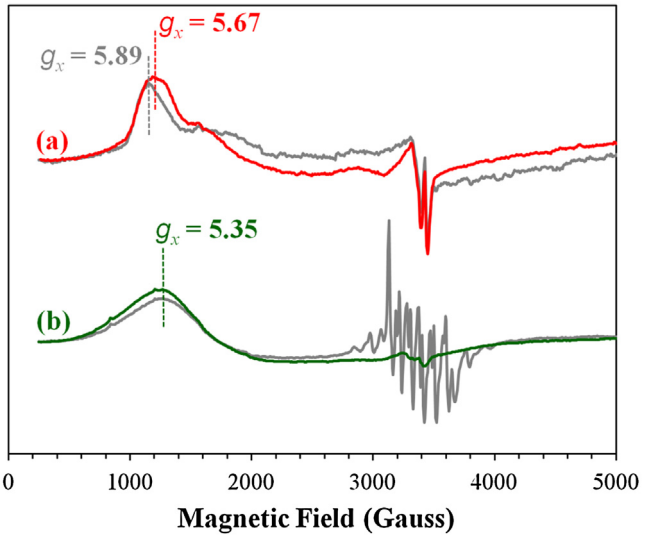

Fig. 9. X-band EPR spectra of (a) Co^{III}(cyclam)X/P25 and (b) Co^{III}(cyclam)X/Rutile under CO_2. Corresponding spectra under N_2 are also included (gray traces). The spectra were collected at liquid He temperature.

region consisting of a broad Co(II) peak with $g = 5.35$ that suggests averaging of g_x and g_y components indicative of Co(II) in a broad range of coordination geometries. The overall spectrum shows evidence of weakly distinguishable hyperfine structure from the ^{59}Co nuclear spin momentum in a lower field component with a hyperfine coupling of ~350 G. Since Co has a nuclear spin of 7/2 100% abundance, Co hyperfine has eight lines. These spectra are consistent with those expected for $S = 3/2$ molecules subject to zero-field splitting where only the (±1/2) Kramers' doublet is resonant. The hyperfine contribution is much more evident in the region of $g = 2$ where strong eight-line signals are observed. However the hyperfine splitting in this region of the spectrum is much smaller (86 G). The hyperfine splitting of Co(II) is usually in the range between 150 G and 300 G in the low-field region. The small hyperfine coupling and different saturation properties of the signal around g ~2 from the one of high spin Co are consistent with the existence of surface radicals whose EPR transitions split into eight lines due to the presence of ^{59}Co in close proximity. Since the g value is ~2, these transitions are mostly likely associated with oxygen-centered radicals. Close inspection of the spectra shows existence of three sets of eight-line splitting, suggesting the existence of three sets of oxygen-centered radicals with $g = 2.141$, 2.028, and 2.019 (Fig. S7).

Therefore, the Co(II) sites in Co^{III}(cyclam)X/Rutile are in a broad range of coordination geometries different than those in Co^{III}(cyclam)X/P25. Likely, oxygen molecules are coordinated to Co centers in the large aggregates of Co^{III}(cyclam)X deposited on Rutile (Figs. 7 c and d and 8), but not in Co^{III}(cyclam)X/P25 or Co^{III}(cyclam)X/Anatase where the Co sites are molecularly deposited on TiO_2 surfaces through Ti—O—Co linkages (Fig. 1).

The adsorption of CO_2 on the hybrid photocatalysts was carried out by exposing the samples to CO_2 at room temperature and then freezing the samples at liquid He temperature prior to collecting EPR spectra. Binding of CO_2 to the Co(II) sites in Co^{III}(cyclam)X/P25 shifted the high-spin signal from $g_x = 5.89$ to $g_x = 5.67$ (Fig. 9a). The comparison between the Co(II) resonances observed for Co^{III}(cyclam)X/P25 is very similar to that between Co(II) sites in zeolite frameworks without and with calcinations at elevated temperatures [60,61]. In particular, a Co(II) signal around $g_x = 5.80$ was observed in the EPR spectrum of a cobalt-containing microporous aluminophosphate. The Co(II) signal shifted to $g_x = 5.44$ upon calcination of the microporous material, which induced changes in the coordination geometry of the Co(II) accompanied with shortening of Co—O bond [60]. Therefore, our observation indicates that CO_2 upon adsorption on Co^{III}(cyclam)X/P25 took electron density away from the Co(II) centers, either directly or indirectly by interacting with neighboring Ti(IV) sites shifting the g value towards higher fields. In Co^{III}(cyclam)X/Rutile (Fig. 9b), binding of CO_2 did not change the high-spin Co(II) signal at $g_x = 5.35$. Instead, the hyperfine splitting of the oxygen radicals vanished and an anisotropic signal appeared near $g = 2$ (not labeled). This observation implies that the electron density on the oxygen radicals adjacent to Co(II) was preferentially transferred to CO_2 and adsorption of CO_2, in fact, removed electron exchange of Co(II) with oxygen atoms on the Rutile surface.

The results shown in Fig. 8 provide important insights regarding the coordination geometry of Co(II) centers as well as interaction of CO_2 with the surface Co(II) sites. Most likely, the coordination geometry of surface Co(III) sites in Co^{III}(cyclam)X/Rutile is also different than that in Co^{III}(cyclam)X/P25 and Co^{III}(cyclam)X/Anatase. Further studies are underway to probe CO_2 reduction under photochemical conditions with EPR spectroscopy.

4. Conclusions

In summary, we have synthesized hybrid photocatalysts by depositing a macrocyclic Co(III) complex on three different TiO_2 nanomaterials *via* a microwave method. In the presence of triethanolamine as an electron donor, TiO_2 nanoparticles were activated upon UV irradiation and transferred electrons to the surface Co(III) catalyst for CO_2 reduction. Experimental results based on UV–vis and infrared spectroscopy and transmission electron microscopy indicate that catalytically active Co(III) sites were molecularly deposited on TiO_2 surfaces through reacting with terminal OH groups. In the absence of such terminal OH groups, the Co(III) complex formed amorphous aggregates on TiO_2 nanoparticles. Molecularly deposited Co(III) sites demonstrated significantly higher activity than aggregates of the Co(III) complex in photocatalytic CO_2 reduction because of efficient interfacial electron transfer from photoactivated TiO_2 to the former. Further studies with electron paramagnetic resonance spectroscopy indicated the presence of paramagnetic Co(II) species in the synthesized hybrid photocatalysts. The spectroscopic investigation also revealed important differences in the coordination geometry and interactions with CO_2 of the Co(II) sites between the molecularly deposited and aggregated cobalt sites. Our results highlight the importance of surface characteristics in the fabrication of hybrid photocatalysts consisting of molecular complexes on metal oxide surfaces.

Acknowledgments

This research conducted at the University of New Hampshire was supported by the U.S. National Science Foundation through grant CBET-1510810 to G.L. The EPR work was performed at Argonne National Laboratory, the Center for Nanoscale Materials, a U.S. Department of Energy, Office of Science, Office of Basic Energy Sciences User Facility under Contract No. DE-AC02-06CH11357. The generous donation of P25 TiO_2 by Evonik is greatly appreciated. We are grateful to Drs. Alexander Cowan, Richard Johnson, and Scott Greenwood for helpful discussions and assistance in various aspects of experiments.

Appendix A. Supplementary data

Supplementary data associated with this article can be found, in the online version, at http://dx.doi.org/10.1016/j.molcata.2016.07.019.

References

[1] A.M. Appel, J.E. Bercaw, A.B. Bocarsly, et al., Chem. Rev. 113 (2013) 6621–6658.
[2] M. Mikkelsen, M. Jorgensen, F.C. Krebs, Energy Environ. Sci. 3 (2010) 43–81.
[3] Y. Yamazaki, H. Takeda, O. Ishitani, J. Photochem. Photobiol. C 25 (2015) 106–137.
[4] A.J. Morris, G.J. Meyer, E. Fujita, Acc. Chem. Res. 42 (2009) 1983–1994.
[5] E.E. Benson, C.P. Kubiak, A.J. Sathrum, J.M. Smieja, Chem. Soc. Rev. 38 (2009) 89–99.
[6] J.L. White, M.F. Baruch, J.E. Pander III, et al., Chem. Rev. 115 (2015) 12888–12935.
[7] S.N. Habisreutinger, L. Schmidt-Mende, J.K. Stolarczyk, Angew. Chem. Int. Ed. 52 (2013) 7372–7408.
[8] P.D. Tran, L.H. Wong, J. Barber, J.S.C. Loo, Energy Environ. Sci. 5 (2012) 5902–5918.
[9] C.D. Windle, E. Reisner, Chimia 69 (2015) 435–441.
[10] M.E. Louis, T.G. Fenton, J. Rondeau, T. Jin, G. Li, Comments Inorg. Chem. 36 (2016) 38–60.
[11] C. Liu, K.D. Dubois, M.E. Louis, A.S. Vorushilov, G. Li, ACS Catal. 3 (2013) 655–662.
[12] T.G. Fenton, M.E. Louis, G. Li, J. Mol. Catal. A 411 (2016) 272–278.
[13] Y. Ueda, H. Takeda, T. Yui, K. Koike, Y. Goto, S. Inagaki, O. Ishitani, ChemSusChem 8 (2015) 439–442.
[14] M.L. Macnaughtan, H.S. Soo, H. Frei, J. Phys. Chem. C 118 (2014) 7874–7885.
[15] J.-L. Wang, C. Wang, W. Lin, ACS Catal. 2 (2012) 2630–2640.
[16] H. Takeda, M. Ohashi, T. Tani, O. Ishitani, S. Inagaki, Inorg. Chem. 49 (2010) 4554–4559.
[17] K. Maeda, K. Sekizawa, O. Ishitani, Chem. Commun. 49 (2013) 10127–10129.
[18] T. Arai, S. Tajima, S. Sato, K. Uemura, T. Morikawa, T. Kajino, Chem. Commun. 47 (2011) 12664–12666.
[19] C. Wang, Z. Xie, K.E. deKrafft, W. Lin, J. Am. Chem. Soc. 133 (2011) 13445–13454.
[20] C.L. Anfuso, R.C. Snoeberger III, A.M. Ricks, W. Liu, D. Xiao, V.S. Batista, T. Lian, J. Am. Chem. Soc. 133 (2011) 6922–6925.
[21] T. Jin, C. Liu, G. Li, Chem. Commun. 50 (2014) 6221–6224.
[22] E.-G. Ha, J.-A. Chang, S.-M. Byun, C. Pac, D.-M. Jang, J. Park, S.O. Kang, Chem. Commun. 50 (2014) 4462–4464.
[23] G. Neri, J.J. Walsh, C. Wilson, et al., Phys. Chem. Chem. Phys. 17 (2015) 1562–1566.
[24] C.D. Windle, E. Pastor, A. Reynal, A.C. Whitwood, Y. Vaynzof, J.R. Durrant, R.N. Perutz, E. Reisner, Chem. Eur. J. 21 (2015) 3746–3754.
[25] D.-I. Won, J.-S. Lee, J.-M. Ji, W.-J. Jung, H.-J. Son, C. Pac, S.O. Kang, J. Am. Chem. Soc. 137 (2015) 13679–13690.
[26] R. Kuriki, K. Sekizawa, O. Ishitani, K. Maeda, Angew. Chem. Int. Ed. 54 (2015) 2406–2409.
[27] T. Jin, C. Liu, G. Li, J. Coord. Chem. 69 (2016) 1748–1758.
[28] T. Inoue, A. Fujishima, S. Konishi, K. Honda, Nature 277 (1979) 637–638.
[29] G. Li, K.A. Gray, Chem. Phys. 339 (2007) 173–187.
[30] N.M. Dimitrijevic, B.K. Vijayan, O.G. Poluektov, T. Rajh, K.A. Gray, H.-Y. He, P. Zapol, J. Am. Chem. Soc. 133 (2011) 3964–3971.
[31] D. Finkelstein-Shapiro, S.H. Petrosko, N.M. Dimitrijevic, D. Gosztola, K.A. Gray, T. Rajh, P. Tarakeshwar, V. Mujica, J. Phys. Chem. Lett. 4 (2013) 475–479.
[32] L. Liu, Y. Li, Aerosol Air Qual. Res. 14 (2014) 453–469.
[33] D.C. Hurum, A.G. Agrios, K.A. Gray, T. Rajh, M.C. Thurnauer, J. Phys. Chem. B 107 (2003) 4545–4549.
[34] D.C. Hurum, K.A. Gray, T. Rajh, M.C. Thurnauer, J. Phys. Chem. B 109 (2005) 977–980.
[35] G. Li, N. Dimitrijevic, L. Chen, J. Nichols, T. Rajh, K.A. Gray, J. Am. Chem. Soc. 130 (2008) 5402–5403.
[36] M.R. Hoffmann, J.A. Moss, M.M. Baum, Dalton Trans. 40 (2011) 5151–5158.
[37] H. He, C. Liu, K.D. Dubois, T. Jin, M.E. Louis, G. Li, Ind. Eng. Chem. Res. 51 (2012) 11841–11849.
[38] S. Navalon, A. Dhakshinamoorthy, M. Alvaro, H. Garcia, ChemSusChem 6 (2013) 562–577.
[39] B. O'Regan, M. Grätzel, Nature 353 (1991) 737–740.
[40] M. Grätzel, Nature 414 (2001) 338–344.
[41] G.J. Meyer, Inorg. Chem. 44 (2005) 6852–6864.
[42] G. Li, C. Richter, R.L. Milot, L. Cai, C.A. Schmuttenmaer, R.H. Crabtree, G.W. Brudvig, V.S. Batista, Dalton Trans. (2009) 10078–10085.
[43] G.J. Meyer, ACS Nano 4 (2010) 4337–4343.
[44] J.H. Alstrum-Acevedo, M.K. Brennaman, T.J. Meyer, Inorg. Chem. 44 (2005) 6802–6827.
[45] W.J. Youngblood, S.-H.A. Lee, Y. Kobayashi, E.A. Hernandez-Pagan, P.G. Hoertz, T.A. Moore, A.L. Moore, D. Gust, T.E. Mallouk, J. Am. Chem. Soc. 131 (2009) 926–927.
[46] Z. Chen, J.J. Concepcion, J.W. Jurss, T.J. Meyer, *2009*, J. Am. Chem. Soc. 131 (*2009*) 15580–15581.
[47] G. Li, E.M. Sproviero, W.R. McNamara, R.C.I. Snoeberger, R.H. Crabtree, G.W. Brudvig, V.S. Batista, *2010*, J. Phys. Chem. B 114 (*2010*) 14214–14222.
[48] W. Song, Z. Chen, M.K. Brennaman, J.J. Concepcion, A.O.T. Patrocinio, N.Y.M. Iha, T.J. Meyer, Pure Appl. Chem. 83 (2011) 749–768.
[49] Y. Zhao, J.R. Swierk, J.D. Megiatto, Jr., et al., Proc. Natl. Acad. Sci. U. S. A. 109 (2012) 15612–15616 (S15612/1-S15612/8).
[50] T.W. Woolerton, S. Sheard, E. Reisner, E. Pierce, S.W. Ragsdale, F.A. Armstrong, J. Am. Chem. Soc. 132 (2010) 2132–2133.
[51] F. Lakadamyali, E. Reisner, Chem. Commun. 47 (2011) 1695–1697.
[52] T. Ogata, S. Yanagida, B.S. Brunschwig, E. Fujita, J. Am. Chem. Soc. 117 (1995) 6708–6716.
[53] T. Ogata, Y. Yamamoto, Y. Wada, K. Murakoshi, M. Kusaba, N. Nakashima, A. Ishida, S. Takamuku, S. Yanagida, J. Phys. Chem. 99 (1995) 11916–11922.
[54] H. He, C. Liu, M.E. Louis, G. Li, J. Mol. Catal. A 395 (2014) 145–150.
[55] K.D. Dubois, A. Petushkov, E.G. Cardona, S.C. Larsen, G. Li, *2012*, J. Phys. Chem. Lett. 3 (*2012*) 486–492.
[56] E. Finocchio, T. Montanari, C. Resini, G. Busca, J. Mol. Catal. A 204–205 (2003) 535–544.
[57] B. Kumar, M. Llorente, J. Froehlich, T. Dang, A. Sathrum, C.P. Kubiak, Annu. Rev. Phys. Chem. 63 (2012) 541–569.
[58] T. Petsi, G.D. Panagiotou, C.S. Garoufalis, C. Kordulis, P. Stathi, Y. Deligiannakis, A. Lycourghiotis, K. Bourikas, Chem. Eur. J. 15 (2009) 13090–13104.
[59] M. Kohno, H. Ohya-Nishiguchi, K. Yamamoto, T. Sakurai, Bull. Chem. Soc. Jpn. 57 (1984) 932–937.
[60] B.M. Weckhuysen, A.A. Verberckmoes, M.G. Uytterhoeven, F.E. Mabbs, D. Collison, E. de Boer, R.A. Schoonheydt, J. Phys. Chem. B 104 (2000) 37–42.
[61] V. Kurshev, L. Kevan, D.J. Parillo, C. Pereira, G.T. Kokotailo, R.J. Gorte, J. Phys. Chem. 98 (1994) 10160–10166.